

Simulation of Traveling Wave Toner Transport Considering Air Drag

Masataka Maeda

Graduate School of Science and Engineering, Ibaraki University, 4-12-1 Nakanarusawa-cho, Hitachi, Ibaraki 316-8511, Japan

Katsuhiro Maekawa

The Research Center for Superplasticity, Ibaraki University, 4-12-1 Nakanarusawa-cho, Hitachi, Ibaraki 316-8511, Japan

Manabu Takeuchi

Department of Electrical and Electronic Engineering, Ibaraki University, 4-12-1 Nakanarusawa-cho, Hitachi, Ibaraki 316-8511, Japan

Abstract. A simulation method to analyze the behavior of a toner cloud driven by a traveling electrostatic wave with air drag is proposed. The two-fluid flow model, which regards air and toner cloud as incompressible and viscous fluids, is employed. A method of the calculation of the electric potential using the moving particle semi-implicit (MPS) method, which is often used in the study of fluid dynamics, is developed in this article. In the present method, all of the motion of the toner, the airflow, and the electric potential are calculated by using the moving particle semi-implicit method. Common calculation points are used in the electrostatic calculation, the toner motion calculation, and the airflow calculation in order to avoid the complexity of data exchange among those calculations. The validity of the calculation of the electric potential using the MPS method is confirmed by comparing the results to those of a model that has a known strict solution. Modeling of the behavior of toner cloud in toner transport with a traveling electrostatic wave is performed. An increase in the maximum synchronous frequency due to air drag is demonstrated. © 2007 Society for Imaging Science and Technology.

[DOI: 10.2352/J.ImagingSci.Technol.(2007)51:5(431)]

INTRODUCTION

Since Masuda et al.¹ demonstrated that powders could be transported by means of a traveling wave of an electric field, the method has been studied in various applications. In electrophotography, theoretical and experimental studies of toner transport have been made using this method. Melcher et al.²⁻⁴ and Schmidlin^{5,6} provided much insight into the understanding of the different modes of toner transport with a traveling electrostatic wave. Numerical analysis of toner transport has also been improved. In early studies, the numerical analyses focused on the motion of a single particle to avoid the complexity of the interaction between particles. In recent years, the motion of many particles has been analyzed. By using the particle-in-cell method for many particle systems, Gartstein and Shaw⁷ showed that the velocity of

particle flow could vary all the way from zero to the phase velocity of the traveling wave. Kober⁸ numerically solved the equations of toner motion by superimposing the electric field due to toner charge and image charge on the electric field applied by the electrodes.

These analyses provided insight into the behavior of large ensembles of toner particles. However, the calculation of the motion of the toner and the electric field was complicated by the dual approach of using both mesh and particle. The motion of the toner is calculated using particles, but the electric field is calculated using a mesh. The variables are calculated independently and must be interpolated between the mesh and the particles at each time step. Moreover, in a many-particle system, the motion of air dragged by the toner particles is not negligible. In many previous numerical analyses of the traveling wave toner transport, the air was supposed to be quiescent and the motion of the air caused by particle motion was not taken into account. A calculation method that not only simplifies the calculation of electric field but also includes the air effect is required.

In order to avoid the complexity of the calculation, we use calculation points that move with the toner or air rather than fixed meshes or grids. This technique makes the calculation of electric field associated with the moving charge and moving air more manageable. The smoothed particle hydrodynamics (SPH) method and the moving particle semi-implicit (MPS) method, which are often used in the study of fluid dynamics, are well-known modeling methods that use moving particles.

In this paper, we propose a simulation method that can solve the problem of toner and air motions and electric field, simultaneously, using a particle method. Using the present method, we calculate the toner motion in traveling wave toner transport and show an overview of the behavior of toner cloud that is affected by airflow as the speed of traveling wave increases.

MODEL

Physical Model

Let us consider the motion of charged toner particles driven by a traveling electrostatic wave taking into account the effect of air motion. We examine the effect of electrostatic force and airflow as a major factor of basic driving mechanism of toner transport with traveling wave.

The electric potential ϕ formed by toner charge is given

$$\nabla \cdot (\varepsilon \nabla \phi) = Q, \quad (1)$$

where ε is the permittivity of media and Q is the space charge density due to toner charge. The electric field can be expressed as

$$\mathbf{E} = -\nabla \phi. \quad (2)$$

In the analysis of a solid-gas flow, such as motion of toner particles in air, the flow structure is different according to whether the particulate phase is dispersed in a fluid phase or separated from a fluid phase. It was reported that toner particles are transported in bands that are spaced by the wavelength of traveling wave.⁴ Therefore, the objective of our method to be developed is to obtain an overview of the behavior of a cluster of toner particles rather than of a discrete toner particle. We regard a cluster of toner particles in a band as a separated phase and as an incompressible fluid. In other words, we employ the two-fluid flow model of air and toner cloud in this study.

From mass and momentum conservation and incompressibility, the equations for air are

$$\frac{D\rho_a}{Dt} = 0, \quad (3)$$

$$\frac{D\mathbf{u}_a}{Dt} = -\frac{1}{\rho_a} \nabla P_a + \nu_a \nabla^2 \mathbf{u}_a + \mathbf{g} - \frac{1}{\rho_a} \mathbf{F}_{at}, \quad (4)$$

$$\mathbf{F}_{at} = -\left(-\frac{1}{\rho_a} \nabla P_a + \nu_a \nabla^2 \mathbf{u}_a \right). \quad (5)$$

The equations for toner cloud are

$$\frac{D\rho_t}{Dt} = 0, \quad (6)$$

$$\frac{D\mathbf{u}_t}{Dt} = -\frac{1}{\rho_t} \nabla P_t + \nu_t \nabla^2 \mathbf{u}_t + \frac{1}{\rho_t} Q\mathbf{E} + \mathbf{g} + \frac{1}{\rho_t} \mathbf{F}_{ta}, \quad (7)$$

$$\mathbf{F}_{ta} = \left(-\frac{1}{\rho_t} \nabla P_t + \nu_t \nabla^2 \mathbf{u}_t \right)_a, \quad (8)$$

where \mathbf{u} is velocity, ρ is density and ν is viscosity of air and toner cloud. Subscript a , t denote air and toner cloud, respectively. Q is volume charge density of toner cloud, and \mathbf{E} is electric field. \mathbf{F}_{at} is the interaction force that is exerted on

air by pressure and viscosity of toner cloud. \mathbf{F}_{ta} is the interaction force that is exerted on toner cloud by pressure and viscosity of air. D/Dt is denotes the Lagrangian time derivative. Since we discretize these equations using a calculation point, as discussed later, these are described as calculation points for air and toner, not for a volume. Thus, the concentration of toner cloud is not expressed in the equations.

Numerical Model

In order to avoid the complicated procedure of interpolating between grid and particle, only calculation points are employed in the calculation of the electric field, motion of toner, and airflow. Mesh and grid are not employed in this study. The calculation points are placed evenly in an analysis area. A toner particle corresponds to one calculation point. The calculation points assigned for toner particles move with the motion of the toner cloud. In order to calculate the electric field, the airflow, and the flow of toner cloud, we examined the particle methods, such as the SPH method and the MPS method, which are usually used for fluid analysis. The SPH method was used to calculate electric potential in our previous study,⁹ but this method requires special schemes to treat incompressible fluid.¹⁰ In the present study, the MPS method,¹¹ which is often used in studies of incompressible flow, is employed the calculation of the electric field. The calculation points assigned for air also move with the airflow calculated using the MPS method.

In the MPS method, calculation points (also called particles in the MPS method) with the physical quantity f are placed evenly in an analysis area. The gradient of the physical quantity f is modeled as the average slope weighted with a weighting function between the object calculation point i and its neighboring calculation points j , and is expressed at a position of calculation point i as

$$\langle \nabla f \rangle_i = \frac{d}{n^0} \sum_{j \neq i} \left[\frac{f_j - f_i}{r_{ij}} \frac{\mathbf{r}_{ij}}{r_{ij}} w(r_{ij}) \right], \quad (9)$$

$$(\mathbf{r}_{ij} = \mathbf{r}_j - \mathbf{r}_i, \quad r_{ij} = |\mathbf{r}_{ij}|),$$

where \mathbf{r}_i is the position vector of calculation point i , and d is the spatial dimension. The weight function w uses the following function:

$$w(r) = \begin{cases} \frac{r_e - r}{r} - 1 & (0 < r \leq r_e) \\ 0 & (r_e > r) \end{cases}, \quad (10)$$

where r_e is the size of weight function that defines interacting calculation points and n^0 is the number density of calculation points in the initial configuration, and is defined by

$$n^0 = \sum_{j \neq i} w(r_{ij}). \quad (11)$$

The Laplacian is modeled as

$$\langle \nabla^2 f \rangle_i = \frac{2d}{n^0 \lambda} \sum_{j \neq i} [(f_j - f_i) w(r_{ij})], \quad (12)$$

where

$$\lambda = \frac{\int_V w(r) r^2 d\nu}{\int_V w(r) d\nu}. \quad (13)$$

In order to discretize Eq. (1) for the electric potential using the MPS Laplacian model, Eq. (12), we use the identity

$$\nabla \cdot (\varepsilon \nabla \phi) = \frac{1}{2} [\nabla^2 (\varepsilon \phi) - \phi \nabla^2 \varepsilon + \varepsilon \nabla^2 \phi], \quad (14)$$

and we can obtain the discretization of Eq. (1) as

$$\langle \nabla \cdot (\varepsilon \nabla \phi) \rangle_i = \frac{d}{\lambda n^0} \sum_{j \neq i} [(\varepsilon_j + \varepsilon_i)(\phi_j - \phi_i) w(r_{ij})] = -Q_i. \quad (15)$$

Solving Eq. (15) simultaneously for unknown ϕ with the charge density and the boundary potential we obtain the potential at each calculation point. Here, the charge densities Q_i are given as a property of the calculation points for toner, and the boundary potentials are given as a property of the calculation points at the boundary. From Eq. (9), the electric field is obtained by

$$\langle E \rangle_i = -\langle \nabla \phi \rangle_i = -\frac{d}{n^0} \sum_{j \neq i} \left[\frac{\phi_j - \phi_i}{r_{ij}} \frac{\mathbf{r}_{ij}}{r_{ij}} w(r_{ij}) \right]. \quad (16)$$

Two-fluid flow of toner cloud flow and airflow is discretized by calculation points with toner mass and calculation points with air mass, respectively, in MPS. The continuity equations [Eqs. (3) and (6)] are satisfied by keeping the number of calculation points constant during the motion in the analysis area. Keeping the number density of the calculation points constant, n^0 satisfies the incompressibility. The Navier–Stokes equations [Eqs. (4) and (7)] are calculated as follows.¹²

In a time step k , the terms with the exception of the pressure term of Eqs. (4) and (7) are explicitly calculated, and temporal velocities \mathbf{u}^* are obtained as

$$\mathbf{u}_a^* = \mathbf{u}_a^k + \left[\left(\frac{\mu_a}{\rho_a} \nabla^2 \mathbf{u}_a \right)_a + \left(\frac{\mu_a}{\rho_a} \nabla^2 \mathbf{u}_a \right)_t + \mathbf{g} \right] \Delta t, \quad (17)$$

$$\mathbf{u}_t^* = \mathbf{u}_t^k + \left[\left(\frac{\mu_t}{\rho_t} \nabla^2 \mathbf{u}_t \right)_t + \left(\frac{\mu_t}{\rho_t} \nabla^2 \mathbf{u}_t \right)_a + \mathbf{g} + \frac{QE}{\rho_t} \right] \Delta t. \quad (18)$$

In Eqs. (17) and (18), $(\)_a$ and $(\)_t$ denote interactions from air and toner, respectively. Temporal positions \mathbf{r}^* are obtained as

$$\mathbf{r}_a^* = \mathbf{r}_a^k + \mathbf{u}_a^* \Delta t \quad (19)$$

$$\mathbf{r}_t^* = \mathbf{r}_t^k + \mathbf{u}_t^* \Delta t \quad (20)$$

where Δt is time step. The viscous term is calculated as

$$\langle \mu \nabla^2 \mathbf{u} \rangle_i = \mu \frac{2d}{\lambda n^0} \sum_{j \neq i} [(\mathbf{u}_j - \mathbf{u}_i) w(r_{ij})]. \quad (21)$$

Since temporal velocities \mathbf{u}^* do not take the pressure term into account, the velocities of the next step $k+1$, \mathbf{u}^{k+1} should be corrected as follows:

$$\mathbf{u}_a^{k+1} = \mathbf{u}_a^* + \mathbf{u}'_a, \quad (22)$$

$$\mathbf{u}_t^{k+1} = \mathbf{u}_t^* + \mathbf{u}'_t, \quad (23)$$

where \mathbf{u}' are the correction velocities. The correction velocities \mathbf{u}' due to the pressure term can be written as

$$\mathbf{u}'_a = - \left[\left(\frac{1}{\rho_a} \nabla P_a^{k+1} \right)_a + \left(\frac{1}{\rho_a} \nabla P_a^{k+1} \right)_t \right] \Delta t, \quad (24)$$

$$\mathbf{u}'_t = - \left[\left(\frac{1}{\rho_t} \nabla P_t^{k+1} \right)_t + \left(\frac{1}{\rho_t} \nabla P_t^{k+1} \right)_a \right] \Delta t. \quad (25)$$

The first and second terms on the right-hand side of Eq. (24) denote pressure gradients due to interactions neighboring calculation points for air and toner, respectively. Adding both sides of Eqs. (24) and (25) gives

$$(1-c) \frac{\mathbf{u}'_a}{\Delta t} + c \frac{\rho_t \mathbf{u}'_t}{\rho_a \Delta t} = - \frac{1}{\rho_a} \nabla P^{k+1},$$

$$\nabla P^{k+1} = (1-c)[(\nabla P_a)_a + (\nabla P_a)_t] + c[(\nabla P_t)_t + (\nabla P_t)_a], \quad (26)$$

where c is concentration of toner.

Since the temporal position \mathbf{r}^* does not satisfy the incompressibility constraint, that is to say, the temporal number density of calculation point at the temporal position n^* is not n^0 . The temporal number density of calculation point n^* should be corrected to n^0 as

$$n^0 = n^* + n', \quad (27)$$

where n' is the corrected value of the calculation point number density. The correction value of calculation point number density n' is related to the velocity correction \mathbf{u}' through the mass conservation equation.

$$\frac{n'}{n^0 \Delta t} + \nabla \cdot \left((1-c) \mathbf{u}'_a + c \frac{\rho_t}{\rho_a} \mathbf{u}'_t \right) = 0. \quad (28)$$

With Eqs. (26)–(28), Poisson equations of pressure are obtained as

$$\nabla^2 P_a^{k+1} = \frac{\rho_a}{\Delta t^2} \frac{n^* - n^0}{n^0}, \tag{29}$$

$$\nabla^2 P_t^{k+1} = \frac{\rho_t}{\Delta t^2} \frac{n^* - n^0}{n^0}. \tag{30}$$

From Eq. (12), we obtain

$$\frac{2d}{n^0 \lambda} \sum_{j \neq i} [(P_j - P_i) w(r_{ij})] = - \frac{\rho_m}{\Delta t^2} \frac{n_i^* - n^0}{n^0} \quad m = a, t. \tag{31}$$

Solving the simultaneous equations [Eq. (31)] for unknowns P gives the pressure at each calculation point. With Eq. (9), the gradient of the pressure is obtained as

$$\langle \nabla P \rangle_i = - \frac{d}{n^0} \sum_{j \neq i} \left[\frac{P_j - P_i}{r_{ij}} \frac{r_{ij}}{r_{ij}} w(r_{ij}) \right]. \tag{32}$$

Finally, the velocities of air and toner at next step $k+1$ are obtained using Eqs. (22)–(25) and (32). Here, the equations for air and toner cloud are described separately in order to point out the interaction between toner cloud and air explicitly. However, the program code can be written in the same way with one flow model using two kinds of densities and two kinds of coefficients of viscosity. As described above, we can obtain the motion of the toner, airflow, and the electric field using only calculation points.

TEST CALCULATIONS

Electric Potential

In order to confirm the validity of the application of the Laplacian model in the MPS method for the calculation of electric potential, we performed a calculation of two cases of potential distribution with and without charge. The first case is an analysis of the gap between parallel plates with sinusoidal potential and ground potential as shown in Figure 1. The analysis area is of width $L=1$ mm, and height $h=0.2$ mm. The potentials applied to the upper and lower plate are

$$\phi_{\text{upper}}(x) = 0, \tag{33}$$

$$\phi_{\text{lower}}(x) = V_0 \sin \left[\frac{2\pi}{\lambda} x \right]. \tag{34}$$

The peak voltage is $V_0=200$ V and the wavelength is $\lambda=L$. The calculation points are placed in a 100×20 matrix. The top and bottom rows of the calculation points are set to

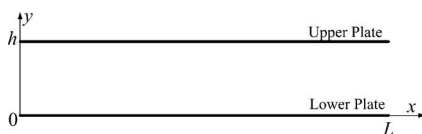


Figure 1. Calculation geometry of parallel plates.

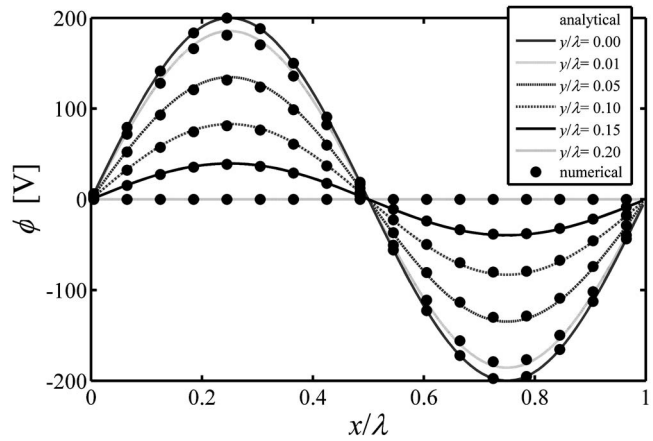


Figure 2. Comparison between numerical solutions by the MPS Laplacian model and analytical solution of the electric potential formed between the parallel plates with applied sinusoidal voltage.

be the potentials ϕ_{upper} and ϕ_{lower} , respectively, as the Dirichlet boundary condition. The periodic boundary condition is applied in the x direction. The size of the weight function is $r_e=2.1l_0$, where l_0 is the distance between neighboring calculation points. Two rows of dummy calculation points are added at the outside of the plates to avoid the error of number density of calculation points near the boundary.

Figure 2 shows a comparison between the numerical results by the present method and the analytical solution. As a whole, the calculated potential is in good agreement with the analytical solution. The maximum error, which is generated near the lower plate, is $<2.5\%$. The error is caused by the fact that in order to simplify the handling of the boundary condition, the boundary condition is located not between calculation points but at the calculation points themselves. The second case is an electric potential analysis that involves toner charge. A toner layer, with depth of 0.035 mm, dielectric permittivity of 2.0, and a charge density of 1.5 C/m^3 , is placed on the lower plate in the geometry as shown in Fig. 1. The potential distribution formed between the parallel plates with potentials of -200 V and 0 V was calculated using the Laplacian model in MPS as represented in Eq. (15). Figure 3 shows a comparison between the numerical results by the present method and the analytical solution. The left vertical dotted line denotes the surface of the toner layer. These results show that the Laplacian model in MPS correctly calculates the electric potential with or without space charge.

Airflow

A test calculation of the airflow caused by the motion of a toner cloud and the force exerted on the surface of toner cloud by air in motion were performed using the present method. To verify the interaction between the airflow and the surface of the toner cloud, insofar as the motion of the toner generates airflow, we used a toner cloud moving with a uniform velocity and a uniform shape. The calculation points representing the toner cloud are placed in the shape of a trapezoid and move at a constant velocity of 0.1 m/s in

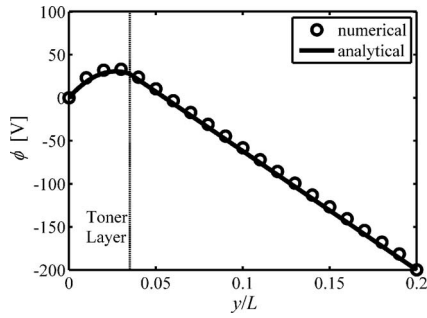


Figure 3. Comparison between numerical solutions by the MPS Laplacian model and the analytical solution of electric potential with toner charge.

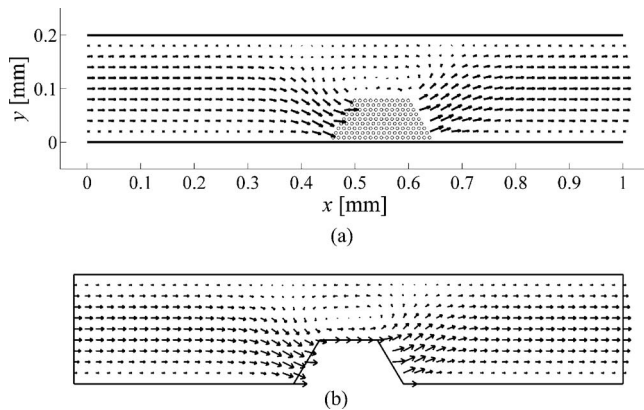


Figure 4. Distribution of velocity of air calculated (a) by the present method and (b) by the FEM method.

the x direction. The analysis area is of width $L=1$ mm, and height $h=0.2$ mm. The periodic boundary condition, whereby the calculation points leaving from one boundary are returned through the other, is applied in the x direction. The air density and viscosity are $\rho=1.205$ kg/m³ and $\mu=1.82 \times 10^{-5}$ Pa s, respectively. The system is initially at rest. The time step used is $\Delta t=1 \times 10^{-6}$ s. The steady state of the same problem is calculated using a commercial finite element method (FEM) code for comparison. In this FEM calculation, the toner cloud is modeled by a boundary of a trapezoidal shape. The boundary condition is the inflow/outflow condition with the velocity of the toner cloud instead of moving the trapezoidal geometry to simulate the motion of toner cloud. The no-slip condition is applied at the upper and lower plates.

Figure 4(a) shows the distribution of the velocity of air at $t=50 \mu\text{s}$ calculated by the present method. Figure 4(b) shows the result of the steady-state condition calculated by the FEM code. The viscous force and pressure acting on the surface of toner cloud by air in motion was calculated using the present method and are shown in Figure 5. The results calculated by FEM are also plotted for comparison.

The velocity field calculated using the present method including the vortex over the trapezoidal shape is in good agreement with the result using the FEM code for the most part. There is a small discrepancy between the present

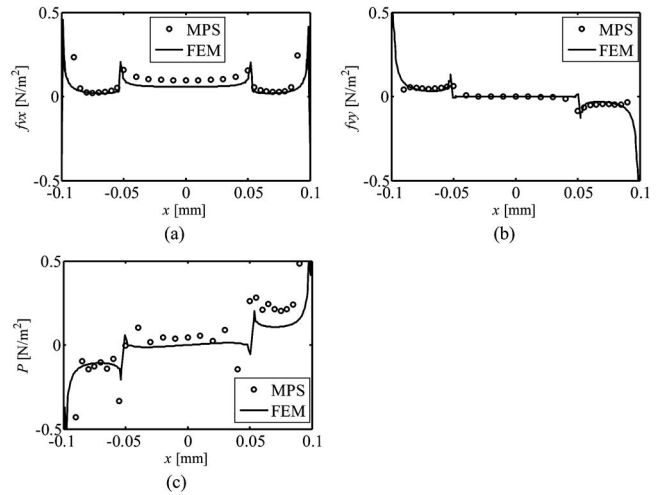


Figure 5. Comparison of results calculated between by the present method and by the FEM method, (a) x -component of viscous force, (b) y -component of viscous force, and (c) pressure that exerted on the surface of a toner cloud in the shape of trapezoid by airflow.

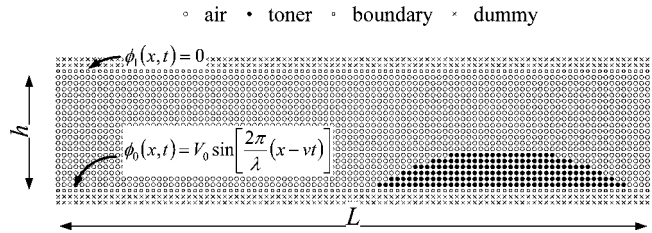


Figure 6. Initial configuration of calculation points for analysis of traveling wave toner transport.

method and the FEM code in calculating the viscous force and the pressure. However, the results are adequate for our qualitative estimate.

TRAVELING WAVE TONER TRANSPORT

The results of the verification tests described above show that the present method is adequate for the calculation of the electric field, the airflow caused by the motion of toner and the viscous force, and the pressure acting on the surface of toner cloud by air in motion. We employed the present method for the analysis of the behavior of a toner cloud transporting with a traveling electrostatic wave.

The initial configuration of the calculation points is shown in Figure 6, and the parameters of the calculation are listed in Table I. The periodic boundary condition is applied in the x direction. The traveling potential applied to the lower plate is as follows:

$$\phi_0(x,t) = V_0 \sin\left[\frac{2\pi}{\lambda}(x - vt)\right], \quad v = \lambda f, \quad (35)$$

where v is the phase velocity.

In our first simulation by the present method, we performed calculations to obtain the frequency characteristics of the transport velocity of the toner. The frequency of the traveling wave is swept from 0 Hz to 3.0 kHz in the period

Table I. Parameters of toner transport model.

Analysis Area	
Width L (m)	1.0×10^{-3}
Height h (m)	0.2×10^{-3}
Pitch of calculation-point l_0 (m)	0.01×10^{-3}
Traveling Electrostatic Wave	
Wavelength λ (m)	1.0×10^{-3}
Applied Voltage V_0 (V)	200
Frequency (kHz)	0–3.0
Toner	
Charge Density Q (C/m ³)	0.3
Relative Permittivity	1.2
Bulk Density ρ_t (kg/m ³)	300
Viscosity μ_t (Pa s)	0
Air	
Relative Permittivity	1.0
Density ρ_a (kg/m ³)	1.2
Viscosity μ_a (Pa s)	1.82×10^{-5}
Time Step	
Step (s)	1.0×10^{-6}
Span (s)	75×10^{-3}
Size of Weight Function	
Electric Potential	$2.1l_0$
Number Density	$2.1l_0$
Pressure	$4.0l_0$

from $t=0$ ms to 75 ms in the calculation. In other words, the phase velocity is varied from 0 ms to 3.0 ms at the wavelength of traveling wave $\lambda=1$ mm. We focus on the effect of electrostatic force and air drag. The viscosity of toner cloud flow is taken to be zero to exclude the effect of friction between toner and the plate, to which the traveling wave potential is applied, and the effect of friction among toner particles.

Figure 7 shows the velocity distribution of the toner particles with airflow caused by the motion of toner as a function of the phase velocity of traveling wave. The solid line in Fig. 7 denotes the phase velocity of the traveling wave, and the dotted lines denote the critical velocity at which the Stokes' force is equal to the electrostatic force of one particle in quiescent air. In Fig. 7, as the wave phase velocity of the traveling wave increases from zero, the toner particles move synchronously with the wave phase velocity until a certain wave phase velocity. Beyond this phase velocity, the number of toner particles that move synchronously with the wave phase velocity decreases gradually with an increase in phase velocity. Finally, the velocities of all toner particles do not synchronize with the wave phase velocity.

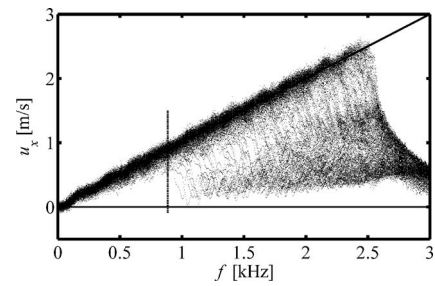


Figure 7. Distribution of toner particle velocity vs phase velocity of traveling wave.

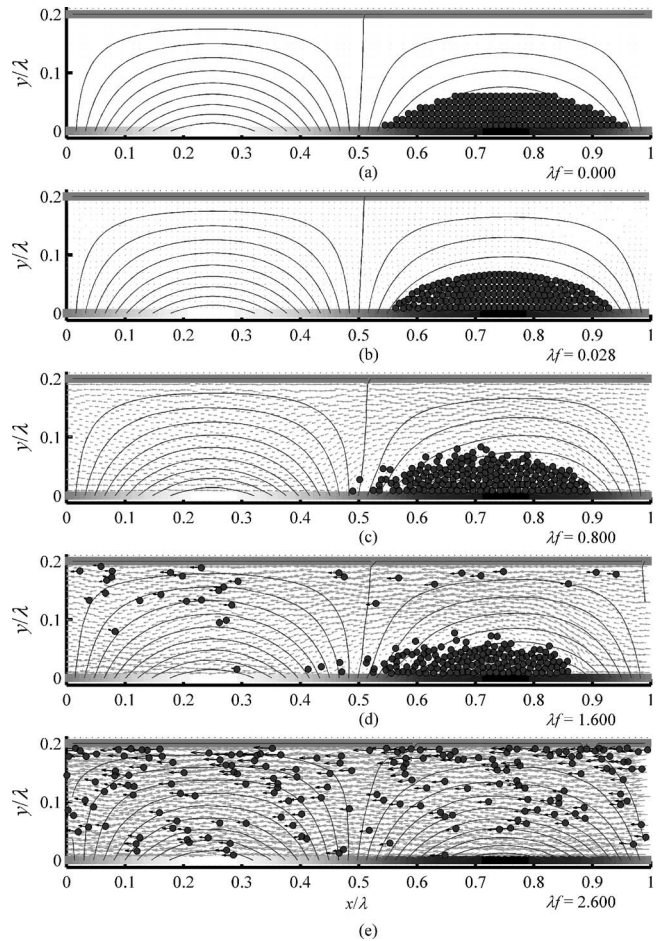


Figure 8. A snapshot of position of toner particles and velocity field of airflow: (a) Initial (starting) step, (b) the step when the toner particles rearrange in response to the electric field, (c) the step when the toner cloud deforms due to air force, (d) the step when part of toner particles separate from the toner cloud due to air force, and (e) the step when all the toner particles are out of phase with the traveling wave and the initial shape of toner cloud disappears.

The motions of toner particles and air were observed as an animation created using the numerical results. Figure 8 shows snapshots of the toner particle position and airflow velocity from the viewpoint of a coordinate moving with the traveling wave. The contour line of the electric potential, which is formed by the traveling wave potential applied on the plate and toner charge, is superimposed. Figure 8(a) shows the positioning of calculation points for toner, which

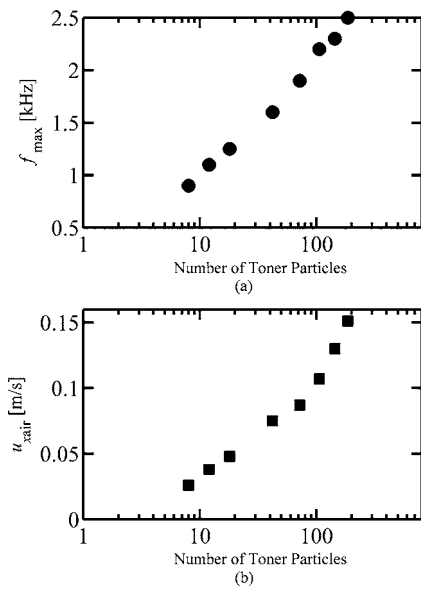


Figure 9. (a) Maximum synchronous frequency as a function of number of toner particles to be transported and (b) average velocity of airflow as a function of number of toner particles to be transported.

are placed in the shape of a chord, geometrically, at the initial step. Figure 8(b) shows the snapshot of the step when the toner particles rearrange in response to the electric field. Figure 8(c) shows the snapshot of the step when the toner cloud deforms due to air force. In Fig. 8(c), the cluster of toner, which is around the trough of potential wave at low velocity in Fig. 8(b), moves to negative direction of x axis due to air resistance. As shown in Fig. 8(d), at higher phase velocity, the airflow around the surface of the cluster of toner causes a separation of the toner particles at the surface of the cluster of toner and the separated toner particles do not move in synchronization with the phase velocity of the traveling wave any longer. Finally, all the toner particles are out of phase of the traveling wave and the initial shape of cluster of toner disappears, as shown in Fig. 8(e).

In our second simulation, we performed calculations of various numbers of toner particles and considered the influence of air drag. Figure 9(a) shows the relationship between the maximum frequency at which the particles move synchronously with the wave phase velocity and the number of toner particles to be transported. Figure 9(b) shows the average airflow velocity in x direction as a function of the number of toner particles. As the number of toner particles increases, the velocity of airflow increases and the maximum synchronous frequency increases.

As mentioned above, we confirmed that air drag caused by toner motion increased the maximum synchronous frequency, at which the toner particles moved synchronously with a phase velocity of a traveling wave.

CONCLUSION

A simulation method to analyze the behavior of a toner cloud driven by a traveling electrostatic wave, taking into account the effect of air motion, is proposed. Several calcu-

lations of traveling wave toner transport using this method were performed. The results demonstrate that airflow dragged by toner particles plays an important role in the behavior of toner particles transporting with a traveling electrostatic wave.

In the traveling wave toner transport, the friction between toner and plate, to which traveling potential is applied, or the friction among toner particles in addition to electrostatic force and air resistance are important. These frictions can be simulated using the viscosity of toner in our two-flow model. Actually, adhesion of charged toner to electrode and cohesion between toner particles occur. We will approach these subjects in the future.

However, the present method calculates the electric potential and the motion of the toner with common calculation points to avoid the complexity of data exchange between the electric potential analysis using meshes or grids and toner motion analysis using particles. This present method allows a direct calculation of the electric potential distribution that varies with the motion of charged toner particle. Moreover, using the same calculation points, airflow can also be calculated. This makes it possible to calculate the behavior of the charged particles in a fluid. The present method can be used to simulate not only toner transport but also in electrophotographic liquid development in which the charged toner moves in a carrier fluid or an electrophoretic paperlike display.

ACKNOWLEDGMENT

The authors are grateful to Chin-Che Tin of Auburn University for his critical reading, kind suggestion, and improvement of the English of this article.

REFERENCES

- S. Masuda, K. Fujibayashi, K. Ishida, and H. Inaba, "Confinement and transport of charged aerosol clouds by means of electric curtains", *Trans. Inst. Electr. Eng. Jpn.*, Part B **92-B**, 9–18 (1972) [in Japanese].
- J. R. Melcher, E. P. Warren, and R. H. Kotwal, "Theory for pure-traveling-wave boundary-guided transport of tribo-electrified particles", *Part. Sci. Technol.* **7**, 1–21 (1989).
- J. R. Melcher, E. P. Warren, and R. H. Kotwal, "Theory for finite-phase traveling-wave boundary-guided transport of triboelectrified particles", *IEEE Trans. Ind. Appl.* **25**, 949–955 (1989).
- J. R. Melcher, E. P. Warren, and R. H. Kotwal, "Traveling-wave delivery of single-component developer", *IEEE Trans. Ind. Appl.* **25**, 956–961 (1989).
- F. W. Schmidlin, "A new nonlevitated mode of traveling wave toner transport", *IEEE Trans. Ind. Appl.* **27**, 480–487 (1991).
- F. W. Schmidlin, "Modes of traveling wave particle transport and their applications", *J. Electrostat.* **34**, 225–244 (1995).
- Y. N. Gartstein and J. G. Shaw, "Many-particle effects in traveling electrostatic wave transport", *J. Phys. D* **32**, 2176–2180 (1999).
- R. Kober, "Simulation of Traveling Wave Toner Transport", *Proc. IS&T's NIP18* (IS&T, Springfield, VA, 2002) pp. 453–457.
- M. Maeda, S. Ozawa, and M. Takeuchi, "Calculation of potential distribution in the vicinity of photoconductive drum and rotating high resistive roller with particle method", *J. Imag. Soc. Jpn.* **45**, 90–96 (2006).
- J. P. Morris, P. J. Fox, and Y. Zhu, "Modeling low Reynolds number incompressible flows using SPH", *J. Comput. Phys.* **136**, 214–226 (1997).
- S. Koshizuka and Y. Oka, "Moving-particle semi-implicit method for fragmentation of incompressible fluid", *Nucl. Sci. Eng.* **123**, 421–434 (1996).
- H. Gotoh, *Computational Mechanics of Sediment Transport* (Morikita Publishing, Tokyo, 2004), p. 110 [in Japanese].